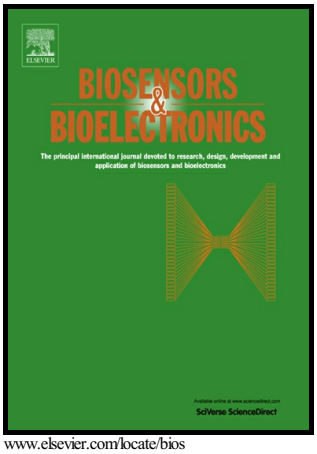

www.elsevier.com/locate/bios

Electrochemical Immunosensors for the Detection of Survival Motor Neuron (SMN) Protein Using Different Carbon Nanomaterials-Modified Electrodes

Shimaa Eissa, Nawal Alshehri, Anas M. Abdel Rahman, Majed Dasouki, Khalid M. Abu Salah, Mohammed Zourob

PII: S0956-5663(17)30674-7
DOI: https://doi.org/10.1016/j.bios.2017.10.015
Reference: BIOS10040

To appear in: *Biosensors and Bioelectronic*

Received date: 25 July 2017
Revised date: 5 October 2017
Accepted date: 9 October 2017

Cite this article as: Shimaa Eissa, Nawal Alshehri, Anas M. Abdel Rahman, Majed Dasouki, Khalid M. Abu Salah and Mohammed Zourob, Electrochemical Immunosensors for the Detection of Survival Motor Neuron (SMN) Protein Using Different Carbon Nanomaterials-Modified Electrodes, *Biosensors and Bioelectronic,* https://doi.org/10.1016/j.bios.2017.10.015

Electrochemical Immunosensors for the Detection of Survival Motor Neuron (SMN) Protein Using Different Carbon Nanomaterials-Modified Electrodes

Shimaa Eissa[a#], Nawal Alshehri[a#], Anas M. Abdel Rahman[a, b], Majed Dasouki[b], Khalid M. Abu Salah[c], Mohammed Zourob[a,b*]

[a] Department of Chemistry, Alfaisal University, Al Zahrawi Street, Al Maather, Al Takhassusi Road, Riyadh 11533, Saudi Arabia

[b] Department of Genetics, King Faisal Specialist Hospital and Research Center, Zahrawi Street, Al Maather, Riyadh 11211, Saudi Arabia.

[c] King Abdullah International Medical Research Center, King Abdulaziz Medical City, Ministry of National Guard, Riyadh, Saudi Arabia.

***Corresponding author:**

E-mail: mzourob@alfaisal.edu

Abstract

Spinal muscular atrophy is an untreatable potentially fatal hereditary disorder caused by loss of function mutations in the survival motor neuron (*SMN*) 1 gene which encodes the SMN protein. Currently, definitive diagnosis relies on the demonstration of biallelic pathogenic variants in *SMN1* gene. Therefore, there is an urgent unmet need to accurately quantify SMN protein levels for screening and therapeutic monitoring of symptomatic newborn and SMA patients, respectively. Here, we developed a voltammetric immunosensor for the sensitive detection of SMN protein based on covalently functionalized carbon nanofiber-modified screen printed electrodes. A comparative study of six different carbon nanomaterial-modified electrodes (carbon, carbon nanotubes, graphene (G), graphene oxide (GO), single wall carbon nanotube (SWCNT), multi-wall carbon nanotube (MWCNT), and carbon nanofiber (CNF)) was performed. 4-carboxyphenyl layers were covalently grafted on the six electrodes by electroreduction of diazonium salt. Then, the terminal carboxylic moieties on the electrodes surfaces were utilized to immobilize the SMN antibody via EDC/NHS chemistry and to fabricate the immunosensors. The electrochemical characterization and analytical performance of the six immunosensors suggest that carbon nanofiber is a better electrode material for the SMN immunosensor. The voltammeric SMN carbon nanofiber-based immunosensor showed high sensitivity (detection limit of 0.75 pg/ml) and selectivity against other proteins such as cystic fibrosis transmembrane conductance regulator (CFTR) and dystrophin (DMD). We suggest that

this novel biosensor is superior to other developed assays for SMN detection in terms of lower cost, higher sensitivity, simplicity and capability of high throughput screening.

Key words: Spinal muscular atrophy (SMA), survival motor neuron (SMN), immunosensor, carbon nanofiber

1. Introduction

Spinal muscular atrophy (SMA) is one of the most common autosomal recessive neurological disorders, affecting around 1 in 6000 births and leading to infant mortality (Farrar and Kiernan 2015). SMA is a hereditary disease results from biallelic (homozygous or compound heterozygous) mutations in the survival motor neuron (*SMN*) gene causing a significant decrease in the expression of the SMN protein. SMA is an anterior horn cell and brain stem nuclei neurodegenerative disease that leads to symmetrical muscle weakness and atrophy which manifests clinically as neonatal hypotonia and may cause death due to respiratory failure. Depending on the disease clinical severity, age of onset, maximum muscular activity achieved, and survivorship, SMA is classified into 4 phenotypes: type 1, severe infantile SMA (Werdnig-Hoffman disease); type II, infantile chronic SMA; type III, juvenile SMA (Wohlfart-Kugelberg-Welander disease); and type IV, adult-onset SMA. While all types of SMA result from recessive mutations in *SMN1*, together, the varying copy number of *SMN2* gene determine the amount of residual SMN protein in the cells and tissues of SMA patients and their clinical phenotype compared to controls (Farrar and Kiernan 2015).

The majority of the therapeutic strategies for SMA aim to increase SMN protein expression. Therefore, there is an urgent need for accurate and sensitive detection assay to monitor the SMN protein levels. Various methods have been used for SMN detection such as

real-time PCR (Liu et al. 2016), denaturing high-performance liquid chromatography (Kao et al. 2006) and mass spectroscopy (Fuller et al. 2015; MacKenzie 2010; Wu et al. 2011). However, these methods are time consuming and require expensive instruments and pre-treatment steps. Several immunoassays have been also developed including enzyme-linked immunosorbent assay (ELISA) (Kobayashi et al. 2011; thi Man et al. 2008), Flow Cytometry (Arakawa et al. 2016), Immunocytochemistry (Coovert et al. 1997; Sangiuolo et al. 2005), Immunofluorescence (Pellizzoni et al. 2001; Rossoll and Bassell 2009), Immunohistochemistry (Chang et al. 2001; Martinez et al. 2012; Monani et al. 2000) and Western Blot (Coovert et al. 1997; Hsieh-Li et al. 2000; Sangiuolo et al. 2005; Wu et al. 2011). Recently, two electrochemiluminescence immunoassays have been developed for SMN detection in whole blood (Zaworski et al. 2016) as well as buccal cells (Steinkellner et al. 2015). However, only few clinical laboratories can carry out these assays because of the long analysis time and high cost.

Few biosensors have appeared recently as alternatives to the traditional assays for SMA diagnosis based on the detection of this gene defect using optical transducers (Chen et al. 2014; Piunno 2009; Watterson et al. 2004). Moreover, SMN protein has been also detected using fiber-optic surface plasmon resonance (SPR) biosensor (Masson et al. 2004). However, the optical biosensors are expensive and SPR cannot be easily miniaturised. Therefore, the development of a cheap, rapid and simple biosensor for SMN detection is still highly desirable.

Electrochemical immunosensors are considered an attractive choice that received considerable attention for protein detection due to their simplicity, sensitivity and capability to undergo miniaturisation. Moreover, the use of screen printed technology has enabled the production of disposable and portable electrodes replacing the conventional electrodes in the biosensor devices. The screen printed electrodes offer several advantages such as the low

production cost, ease of modification and suitability for working with small sample volumes (Lisdat and Schäfer 2008).

Recent advances in the field of nanotechnology have lead to the development of biosensor platforms with improved performance (Cui et al. 2018; Zhou et al. 2015; Ma et al. 2016). The advances in the synthesis of many new nanomaterials with controlled morphologies and unique physicochemical properties have lead to explosion in the biosensor applications (Holzinger et al. 2014). Carbon-based nanomaterials such as carbon nanotubes, graphene (G), graphene oxide (GO), single wall carbon nanotube (SWCNT), multiwall carbon nanotube (MWCNT), and carbon nanofiber (CNF) have been widely utilized in developing electrochemical biosensor platforms (Zhang et al. 2009). Carbon nanomaterials have shown several interesting properties such as high chemical stability, mechanical strength, surface-to-volume ratio and electrical conductivity (Holzinger et al. 2014). These unique properties made them ideal materials for the development of electrochemical biosensors for different applications (Zhang et al. 2009).

One of the most important steps in the biosensor fabrication is the surface modification of the electrode which enables the subsequent immobilization of biomolecules. Electrografting using diazonium salt reduction is among the most common functionalization methods that have been widely studied in different carbon electrodes. This method turned out to be a simple, fast and versatile way for surface modification which leads to covalent attachment of an organic layer to a conductive substrate.

Comparative studies for electrografting of diazonium salts on different substrates have been previously reported. Gooding et al. (Liu et al. 2007) have conducted a comparison of the

effect of carboxyphenyl layers formed on both gold and glass carbon electrodes and their electrochemical sensing application. 4- sulfobenzenediazonium tetrafluoroborate grafting on gold and glass carbon electrodes has also been compared (Liu et al. 2005). The edges and the basal planes of highly oriented pyrolytic graphite have been compared for diazonium electrografting showing faster reaction on the edges than on the basal plane (Kariuki and McDermott 1999).

To the best of our knowledge, no detailed study has been previously reported for comparing the electrografting of diazonium salt on various carbon nanomaterials and their electrochemical biosensing application. In this work, we compare the electrografting using carboxyphenyl diazonium salt reduction on different commercial carbon nanomaterial-modified screen printed electrodes (C, G, GO, CNF, SWCNT, MWCNT). The electron transfer efficiency, defect density and surface chemical composition of the modified electrodes were studied using cyclic voltammetry (CV), Raman spectroscopy and X-ray photoelectron spectroscopy (XPS), respectively. The functionalized electrodes were then used to fabricate label-free electrochemical immunosensors for SMN protein detection and the analytical performance of the different electrode materials was compared.

2. Experimental

2.1.Materials and reagents

Recombinant Human SMN1 protein was purchased from creative Biomart (NY, USA). SMN monoclonal antibody was obtained from Invitrogen (ON, Canada). Potassium ferricyanide ($K_3Fe(CN)_6$) 4-aminobenzoic acid, potassium ferrocyanide ($K_4Fe(CN)_6$), dipotassium hydrogen orthophosphate, sodium chloride, potassium dihydrogen orthophosphate, sodium nitrite, bovine

serum albumin (BSA) and hydrochloric acid were purchased from Sigma (Ontario, Canada). Recombinant human CFTR protein was purchased from Abcam (MA, USA). Dystrophin protein fragment was obtained from Pepmic (Jiangsu, China). N-hydroxysuccinimide (NHS) and 1-ethyl-3-(3-dimethylaminopropyl) carbodiimide hydrochloride (EDC) were purchased from Fisher Scientific (Ontario, Canada). A phosphate buffered saline (PBS) solution (10 mM, pH 5.0) was used for the preparation of the SMN antibody solution for the immobilization step. PBS buffer (10 mM, pH 7.4) was utilised for the preparation of the proteins solutions. A Milli-Q water was used to prepare all the solutions.

2.2.Instrumentation

The CV and SWV electrochemical measurements were recorded using Autolab PGSTAT302N (Eco Chemie, The Netherlands) potentiostat connected to a personal computer and operated by NOVA software 1.11. Six types of disposable screen printed electrodes and electrode connector that enables the connection of the electrode to the potentiostat were purchased from Dropsens, Inc. (Asturias, Spain). The electrodes incorporate a conventional three-electrode configuration, which consists of working electrode (C, SWCNT, MWCNT, G, GO or CNF), carbon counter and silver reference electrodes.

2.3.Procedure

2.3.1. Electrochemical Functionalization of the carbon nanomaterial-modified electrodes and fabrication of the SMN immunosensors

The stepwise modification of the immunosensors is shown in the schematic diagram (scheme 1). First, the 4- carboxyphenyl diazonium salt was *in-situ* prepared by mixing 2 mM 4-aminobenzoic acid solution with 2 mM sodium nitrite solution in 0.5 M HCl and stirring for 5

min at room temperature. Electrografting was used to functionalize the electrodes by electroreduction of the prepared diazonium salt using CV scanning from +0.2 to − 0.6 V at a scan rate of 100 mV s^{-1}. Then, the electrodes were extensively washed with Milli-Q water. The surface characterization was performed by recording the XPS and Raman spectra of the electrodes before and after electrografting. Then, the CP functionalized electrodes were incubated with 100 mM EDC and 20 mM NHS in PBS buffer pH 5.0 for 1 h. Then, the electrodes were washed with PBS buffer pH 5.0 and incubated for 3 h with 50 µL of 10 µg/ml of anti-SMN antibody solution in PBS buffer, pH 7.4 at room temperature in water-saturated atmosphere. The electrodes were then gently rinsed with PBS buffer pH 7.4 to remove the unreacted antibody. Finally, the electrodes were incubated for 30 min with 1 % BSA in PBS buffer, pH 7.4 to block the activated carboxylic groups and the free electrode surface. The immunosensors were then washed with PBS buffer, pH 7.4 and employed for the detection assay or stored at 4°C in PBS buffer, pH 7.4 until further use.

2.3.2. Electrochemical detection measurements

All the detection experiments were performed at room temperature using SWV in 5 mM $[Fe(CN)_6]^{3-/4-}$ redox solution prepared in 10 mM PBS, pH 7.4. The SWV were recorded in the potential range of 0.3 to -0.4 V using the following parameters: a scan rate of 125 mV/s, frequency: 25 Hz, amplitude: 20 mV, interval time: 0.04 s and step potential: -5 mV. Base-line corrections were performed for all the SWV data.

For the immunosensor time optimization experiment, the CNF immunosensors were incubated with SMN protein solution at different time points (10, 15, 20, 25, 30, 45 and 50 min).

Then the sensors were washed and the SWV measurements were recorded in 5 mM $[Fe(CN)_6]^{3-/4-}$ solution.

The detection experiments were performed by incubating 50 µL of different concentration of SMN protein on the working electrode area for 45 min. Then, the electrodes were rinsed with PBS buffer, pH 7.4 containing 0.05% Tween 20 and the SWV measurements were recorded.

For the selectivity experiments, the electrodes were incubated with 50 µL solution of 10 ng/ml of SMN, CFTR, DMD or BSA for 45 min. After washing, the immunosensors were measured using SWV as previously described.

The SMN immunosensor response was determined as the percentage change in the SWV reduction peak current of the $[Fe(CN)_6]^{3-/4}$ redox couple $(i-i^o)/i^o$ %, where i^o is the SWV peak current measured before binding and i is the peak current measured after incubating the SMN immunosensor with different concentrations of SMN or other non specific proteins.

2.3.3. Whole blood samples analysis

The human whole blood sample obtained from a healthy volunteer was subjected to a single freeze-thaw cycle and was then measured using the for SMN immunosensor. The samples were first diluted 1:40 using 10X RIPA (Cell SignalingTech #9806) buffer and then spiked with SMN protein (0.1, 1, 10 ng/ml).

3. Results and discussion

3.1.Scanning electron microscopy characterization of the carbon nanomaterial-modified electrodes

The ease of modification of carbon surfaces with nanomaterials has allowed the large scale production of nanomaterial-modified screen printed electrodes with unique properties for various sensing applications. Here, we compared 6 commercial carbon nanomaterial modified electrodes, their covalent functionalization and utilization as immunosensors for SMN detection. The morphology of the electrode surface of the different materials has been characterized using scanning electron microscopy (SEM) imaging. As shown in Fig. 1, the composition and morphological structure of the electrode surface varies with the material. The graphite carbon electrodes showed a typical multilayer structure. However, the graphene-modified electrodes exhibit a well-packed graphene layered structure with an irregular shape in which the edges of the individual thin sheets can be distinguished. The GO- modified electrodes have shown the characteristic wrinkle morphology of the flexible nano-sheets. On the other hand, it can be clearly seen from the SEM high resolution image that the CNFs have the form of short rods. The MWCNT was uniformly coated on the carbon electrode surface forming a spaghetti-like porous structure. However, SWCNT structures were not obvious in the SEM images likely due to their high packing density on the electrode surface. Thus, it is clear that the special surface morphology of the carbon nanomaterials offer larger surface area than the parent carbon electrodes.

3.2.Cyclic voltammetry functionalization of the various carbon nanomaterial-modified electrodes

The electrografting of the carboxyphenyl film on different carbon surfaces was investigated. The electrografting step was performed by reduction of diazonium salt using CV scanning between 0.4 and -0.6 V. As shown in Fig. 2, single irreversible cathodic peak was observed in the first CV

scan in all the electrodes. These irreversible peaks at potential between -0.2 to -0.3 V were generated from the reduction of the carboxyphenyl diazonium salt via one electron transfer process. The electrochemical reduction leads to the elimination of nitrogen molecule and the formation of an aryl radical that can be grafted to the carbon surface via covalent bond. In the subsequent cycles, decrease in the intensities of the reduction peaks was observed in all six cases. This is attributed to the increase of the number of the grafted carboxyphenyl groups on the carbon material which leads to decrease in the electron transfer efficiency between the diazonium salt and the electrode surface. After a certain number of CV scans, the cathodic peak almost disappeared implying the full coverage of the electrodes surface with the carboxyphenyl film. These observations are in agreement with that previously reported for the electroreduction of diazonium salt on different carbon materials (Eissa et al. 2015; Eissa et al. 2013; Eissa and Zourob 2012; Liu et al. 2005).

One difference between the CVs on the different carbon electrodes is that only one CV cycle was enough to passivate the carbon electrodes. However, double or multiple CV cycles were needed to achieve good coverage on the other carbon nanomaterials. This could be attributed to the larger surface area of the nanomaterial-modified electrodes compared with the graphitic carbon underneath.

3.3.Blocking effect of the grafted carboxyphenyl film on different carbon materials.

After the electrografting step using CV scans, the electrodes were rinsed with water and the SWV measurements were recorded after each CV cycle in $[Fe(CN)_6]^{3-/4-}$. As shown in the supporting information Fig. S1, the SWV cathodic peak current decreased with increasing the number of CV cycles used for the diazonium salt reduction. These results indicate the gradual

blocking effect of the electron transfer by the grafted carboxyphenyl groups. This is likely due to the thickness of the organic layer as well as the negative charge of the terminal carboxylic groups that forms a barrier to the access of the $[Fe(CN)_6]^{3-/4-}$ anions to the electrode surface. Different behavior was also noticeable for the different nanomaterials. For the carbon, SWCNT and MWCNT- modified electrodes, the $[Fe(CN)_6]^{3-/4-}$ reduction peak completely disappeared after the first CV scan indicating full coverage of the surface with the grafted molecules. However, the G, GO and CNF electrodes showed gradual decrease in the peak current with increasing the number of CV cycles and the reduction peak did not disappeared even after multiple CV cycles. Particularly, for the CNF electrodes, the maximum decrease in the current was observed after the first cycle, whereas gradual passivation of the electrode was observed with more CV cycles. These results are consistent with the CV results explained above. It is also well known that a continuous growth of the carboxyphenyl layer to form multilayers can occur with more CV scanning as previously reported (Eissa et al. 2015; Eissa et al. 2013; Eissa and Zourob 2012; Liu et al. 2005).

3.4. Characterization of the electrodes using Raman spectroscopy and XPS

We then examined the electrodes before and after the carboxyphenyl modification using Raman spectroscopy. As shown in the supporting information Fig. S2, the Raman spectra of the bare electrodes showed the characteristic behaviour of the corresponding nanomaterial exhibiting two prominent peaks, a D peak and a G peak. The G and D peaks are associated with the sp^2-hybridised carbon vibrations and sp^3- like defects in the backbone, respectively. We observed enhancement of the D peak intensity after functionalization. This increase indicates the increase in the defect density on the surfaces of the functionalized electrodes because the degree of

disorder in the carbon structure is usually estimated by the ratio between the D and G band intensities (D/G ratio). This increase is due to the breaking of translational symmetry of the honeycomb lattice of C–C sp^2 bonds on the carbon surface due to the formation of localized C–C sp^3 bonds after carboxyphenyl covalent attachment. Moreover, it was noticed that in most cases no further increase of the D peak intensity was seen after the second CV cycle which indicates that 1 CV cycle was enough to cover most of the surface with the grafted molecules. However, in the case of the CNF electrodes, with increasing the number of CV cycles used for the electrografting step, the D/G ratio was gradually increased which was in agreement with the results of the CV and SWV.

The functionalization of the CNF-modified electrodes was also confirmed using XPS. Fig. 3 shows the XPS survey and C1s core level spectra of the bare CNF electrodes before and after functionalization. As expected, the characteristic carbon 1s and oxygen 1s peaks were observed at 284 and 532 eV, respectively. However, after the carboxyphenyl modification, the oxygen level was significantly increased as seen in the survey spectra (Fig 3 A,B). This is attributed to the attachment of the carboxylic groups to the surface. Moreover, a small additional nitrogen 1s peak with a binding energy of 400 eV has also appeared after modification. This nitrogen peak is likely due to the formation of hydrazine by the reaction of the diazonium salt with the hydroxyl groups on the CNF surface as previously reported on other carbon materials (Liu et al. 2005). The high resolution spectra of C1s showed a peak at 288.8 eV, which was typical for the carbon of the grafted carboxylic acid group.

3.5. *Square wave voltammetry characterisation of the CNF-based immunosensor fabrication steps*

SWV was used to characterize the stepwise modification of the immunosensor. The bare CNF electrode exhibited a well-defined cathodic peak. After 4 CV scans, the reduction peak was significantly suppressed indicating the partial blocking of the surface due to the barrier effect caused by the carboxyphenyl film as explained above. Then, after activating the carboxylic groups with EDC/NHS and the immobilization of the SMN antibody, the reduction peak current slightly increased again (Figure S3) presumably due to the neutralization of the negative carboxylic groups with the positive charge of the antibody as previously reported with other immunosensors (Eissa et al. 2013; Eissa et al. 2015; Eissa et al. 2012, Radi et al. 2009). However, after the incubation with the target SMN protein, a further increase in the current was observed. We attribute this to the positive charge of the SMN protein at pH 7.4 (isoelectric point = 8.0 (G1 et al. 1997)) which leads to the attraction of the redox anion to the electrode surface and enhancement of the electron transfer efficiency (Rodriguez et al. 2005).

3.6.Time optimization of SMN immunosensor

In order to achieve the highest immunosensor response signal, the incubation time of the immunosensor with the SMN protein was optimized. Fig. 4A shows the immunosensor response $(i-i^o)/i^o$ % after incubation with SMN protein solution at varying time intervals (10 to 50 min). The sensor response increased with increasing the incubation time with the protein until 45 min. No significant further enhancement in the signal was detected after longer incubation indicating almost maximum binding. Thus, 45 min was chosen as the optimum incubation time for all the subsequent detection experiments.

3.7.Dose response and selectivity of the different carbon nanomaterial-based immunosensor

The SWV technique was used to monitor the binding between the SMN protein and the different immunosensors. The sensor response was monitored by observing the change in the reduction peak current. As shown in Fig. 4B, the different immunosensor responses were compared after incubation with 10 ng/ml SMN protein. It was also very important to study the selectivity of the different immunosensors. In order to do this, each immunosensor was incubated with 2 other non-specific proteins (CFTR and Dystrophin) which normally exist in the blood of healthy people. As shown in Fig. 4B, in all the immunosensors, the response to the non-specific proteins was much lower than the SMN indicating strong selectivity of the sensors. Moreover, it is clear that the CNF immunosensor was the most responsive platform for binding the SMN protein. Therefore, CNF immunosensor was chosen for the subsequent experiments. A comparison of the analytical detection range and detection limits of the five nanomaterials based immunosensors is shown in the supporting information Table S1.

As shown in Fig. 5A, an increase in the SWV reduction peak was observed with different concentrations of SMN (0, 0.001, 0.01, 0.1, 1.0, 10, 100 and 1000 ng mL^{-1}). This increase is due to the positive charge introduced to the electrode surface upon binding of the protein to the antibody as explained above. Good linear relationship was obtained between the sensor response and the logarithm of the SMN concentrations from 1.0 pg ml^{-1} to 100 ng mL^{-1} (Fig. 5B). The linear equation is $(i - i^o)/i^o\% = 198 + 35.9 \log C$ [ng/mL] and R = 0.994. The standard deviations of the measurements were ranging from 5.0 to 7.0 % indicating good reproducibility of the immunosensor. The detection limit (LOD) of the CNF-based immunosensor was calculated to be 0.75 pg mL^{-1}. The limit of detection was calculated as 3 SD/b where SD is the standard deviation of the blank when no analyte is added and the b is slope of the straight line. These results indicate very good sensitivity of the developed assay compared with ELISA and the other

reported immunoassays (Zaworski et al. 2016)(Masson et al. 2004) (Table S2). Moreover, our method offer advantages over the reported ECL and ELISA assays in terms of cost and simplicity. The ECL and ELISA methods were based on sandwich immunoassays which require the use of two antibodies and a secondary labelled antibody for signal generation which increase the number of steps as well as the cost.

The stability of the immunosensor was also tested. The SMN immunosensor signal did not change significantly (about 2 %) after storage for more than one month in buffer at 4 ^{o}C, indicating the stability of the immunosensor.

3.8.Application of the SMN immunosensor in human whole blood

In order to test the applicability of the developed immunosensor in biological samples, we used the immunosensor to detect the endogenous level of SMN in a blood sample from healthy volunteer. After lysing the blood cells with the lysing buffer (1:40), the sample were spiked with standard solutions of SMN protein and assayed using the immunosensor. As shown in Table S3, good recovery percentages were detected for the spiked samples. The calculated endogenous SMN was about 42 ng/ml which was in the range of SMN concentration in other healthy samples detected previously using Electrochemiluminescence immunoassay (Zaworski et al. 2016). These results suggest that the developed immunosensor can be applied for SMA diagnosis using whole blood screening for SMN protein.

4. Conclusion

We have performed for the first time a comparative study for the electrografting of different carbon nanomaterials using reduction of diazonium salt. The functionalized carbon nanomaterials-modified screen printed electrodes were characterized using CV, SWV, XPS,

Raman spectroscopy. Then, the electrodes were used to fabricate label-free immunosensors for SMN protein detection. The immunosensor exploited the direct binding of the SMN protein and the antibody-modified electrode which results in the enhancement of the $[Fe(CN)_6]^{3-/4-}$ redox probe signal due to the positive charge of the protein. It was observed that the CNF immunosensor was the most responsive platform for SMN detection exhibiting also high degree of selectivity against other known non-specific proteins which exist in the blood such as DMD and CFTR. This novel voltammetric CNF-based immunosensor offers a simple, fast, low cost assay platform for SMN detection. The detection limit was 0.75 pg/ml which indicates higher sensitivity of our method than the commercial ELISA kit (LOD= 50 pg/ml) as well as developed assays that used more sophisticated designs. The immunosensor has also shown good recovery percentage when applied in spiked whole blood samples.

Acknowledgments

N.A. Would like to acknowledge KACST for funding under grant number AT – 38 – 78. The authors would like to thank Ms. Sarah Alodan for performing the Raman spectroscopy measurements included in the supporting information file.

References

Arakawa, R., Arakawa, M., Kaneko, K., Otsuki, N., Aoki, R., Saito, K., 2016. Pediatr. Neurol. 61, 70-75.

Chang, J.-G., Hsieh-Li, H.-M., Jong, Y.-J., Wang, N.M., Tsai, C.-H., Li, H., 2001. Proc. Natl. Acad. Sci. 98(17), 9808-9813.

Chen, C.-A., Wang, C.-C., Chen, Y.-L., Jong, Y.-J., Wu, S.-M., 2014. Chem. Comm. 50(59), 8069-8072.

Coovert, D.D., Le, T.T., McAndrew, P.E., Strasswimmer, J., Crawford, T.O., Mendell, J.R., Coulson, S.E., Androphy, E.J., Prior, T.W., Burghes, A.H., 1997. Hum. Mol. Gen. 6(8), 1205-1214.

Cui, L., Li, Y., Lu, M., Tang, B., and Zhang, C.-y., 2018. Biosens. Bioelectron. 99, 1-7.

Eissa, S., Jimenez, G.C., Mahvash, F., Guermoune, A., Tlili, C., Szkopek, T., Zourob, M., Siaj, M., 2015. Nano Res. 8(5), 1698-1709.

Eissa, S., L'Hocine, L., Siaj, M., Zourob, M., 2013. Analyst 138(15), 4378-4384.

Eissa, S., Zourob, M., 2012. Nanoscale 4(23), 7593-7599.

Farrar, M.A., Kiernan, M.C., 2015. Neurotherapeutics 12(2), 290-302.

Fuller, H.R., Mandefro, B., Shirran, S.L., Gross, A.R., Kaus, A.S., Botting, C.H., Morris, G.E., Sareen, D., 2015. Front Cell Neurosci. 9. 506.

Battaglia G, Princivalle A, Forti F, Lizier C, Zeviani M. , 1997. Hum. Mol. Genet. 6, 1961-1971.

Holzinger, M., Le Goff, A., Cosnier, S., 2014. Front. Chem. 2, 63.

Hsieh-Li, H.M., Chang, J.-G., Jong, Y.-J., Wu, M.-H., Wang, N.M., Tsai, C.H., Li, H., 2000. Nat. gen. 24(1), 66-70.

Kao, H.-Y., Su, Y.-N., Liao, H.-K., Liu, M.S., Chen, Y.-J., 2006. Clin. Chem. 52(3), 361-369.

Kariuki, J.K., McDermott, M.T., 1999. Langmiur 15 6534–6540.

Kobayashi, D.T., Olson, R.J., Sly, L., Swanson, C.J., Chung, B., Naryshkin, N., Narasimhan, J., Bhattacharyya, A., Mullenix, M., Chen, K.S., 2011. PLoS One 6(8), e24269.

Lisdat, F., Schäfer, D., 2008. Anal. Bioanal. Chem. 391(5), 1555.

Liu, G., Böcking, T., Gooding, J.J., 2007. J. Electroanal. Chem. 600(2), 335-344.

Liu, G., Liu, J., Böcking, T., Eggers, P.K., Gooding, J.J., 2005. Chem. Phy. 319(1–3), 136-146.

Liu, Z., Zhang, P., He, X., Liu, S., Tang, S., Zhang, R., Wang, X., Tan, J., Peng, B., Jiang, L., 2016. BMC neurology 16(1), 141.

Ma, F., Li, Y., Tang, B., and Zhang, C.-y., 2016. Acc. Chem. Res. 49, 1722-1730.

MacKenzie, A., 2010. Nat. biotechn. 28(3), 235.

Martinez, T.L., Kong, L., Wang, X., Osborne, M.A., Crowder, M.E., Van Meerbeke, J.P., Xu, X., Davis, C., Wooley, J., Goldhamer, D.J., 2012. J Neurosci. 32(25), 8703-8715.

Masson, J.-F., Barnhart, M., Battaglia, T.M., Morris, G.E., Nieman, R.A., Young, P.J., Lorson, C.L., Booksh, K.S., 2004. Analyst 129(9), 855-859.

Monani, U.R., Coovert, D.D., Burghes, A.H., 2000. Hum. Mol. Gen. 9(16), 2451-2457.

Pellizzoni, L., Charroux, B., Rappsilber, J., Mann, M., Dreyfuss, G., 2001. J. Cell Biol. 152(1), 75-86.

Piunno, P.A., 2009. A Reusable Optical Nucleic Acid Biosensor Applied to the Rapid Detection of Single Nucleotide Polymorphisms Associated with Spinal Muscular Atrophy. Discovery medicine.

Radi, A.-E., Munoz-Berbel, X., Lates, V., Marty, J.-L., 2009. Biosens. Bioelectron.24, 1888-1892.

Rodriguez M.C., Kawde A.N., Wang J., 2005. Chem Commun. 14(34):4267-9.

Rossoll, W., Bassell, G.J., 2009. Cell Biology of the Axon, pp. 87-107. Springer.

Sangiuolo, F., Filareto, A., Spitalieri, P., Scaldaferri, M.L., Mango, R., Bruscia, E., Citro, G., Brunetti, E., De Felici, M., Novelli, G., 2005. Hum. Gene Ther. 16(7), 869-880.

Steinkellner, H., Etzler, J., Gmeiner, B.M., Laccone, F., 2015. Assay Drug Dev. Technol. 13(3), 167-173.

thi Man, N., Humphrey, E., Lam, L., Fuller, H., Lynch, T., Sewry, C., Goodwin, P., MacKenzie, A., Morris, G., 2008. Neurology 71(22), 1757-1763.

Watterson, J.H., Raha, S., Kotoris, C.C., Wust, C.C., Gharabaghi, F., Jantzi, S.C., Haynes, N.K., Gendron, N.H., Krull, U.J., Mackenzie, A.E., 2004. Nucleic Acids Res. 32(2), e18-e18.

Wu, C.-Y., Whye, D., Glazewski, L., Choe, L., Kerr, D., Lee, K.H., Mason, R.W., Wang, W., 2011. BMC neuroscience 12(1), 25.

Zaworski, P., von Herrmann, K.M., Taylor, S., Sunshine, S.S., McCarthy, K., Risher, N., Newcomb, T., Weetall, M., Prior, T.W., Swoboda, K.J., Chen, K.S., Paushkin, S., 2016. PLOS ONE 11(3), e0150640.

Zhang, X., Guo, Q., Cui, D., 2009. Sensors 9(2), 1033-1053.

Zhou, J., Yang, Y., and Zhang, C.-y., 2015. Chem.Rev. 115, 11669-11717.

Figure Captions

Fig. 1 (A) Scanning electron microscopy images of the different carbon nanomaterial electrodes (C, G, GO, CNF, SWCNT and MWCNT). The inset figures are the high resolution images.

Fig. 2 Successive CV scans for the *in situ* generated 4-carboxyphenyl diazonium salt in the diazonium mixture (2 mM $NaNO_2$ + 2 mM 4-aminobenzoic acid in 0.5 M HCl) at scan rate of 100 mVs^{-1} on different carbon nanomaterial-modified electrodes, the black lines represent the first CV and the coloured lines represent the subsequent cycles.

Fig. 3 XPS survey spectra and C1s high resolution spectra of the CNF- modified electrodes before and after carboxyphenyl electrografting.

Fig. 4A. CNF immunosensor response with increasing incubation time of the SMN protein; (B) The response signals of the different electrodes towards the binding with SMN, CFTR and DMD.

Fig. 5A. SWV of the CNF immunosensor incubated with different concentrations of SMN (0.001, 0.01, 0.1, 1.0, 10, 100 and 1000 ng mL^{-1}). (B) The calibration curve was based on the change of the SWV peak currents versus the logarithm of the SMN concentrations. The error bars represent the standard deviation of duplicate measurements

Scheme 1 SMN detection scheme: (A) Different carbon nanomaterial-modified screen printed electrodes, (B) functionalizion of the electrodes via diazonium salt reduction and immunosensor fabrication

Fig. 1

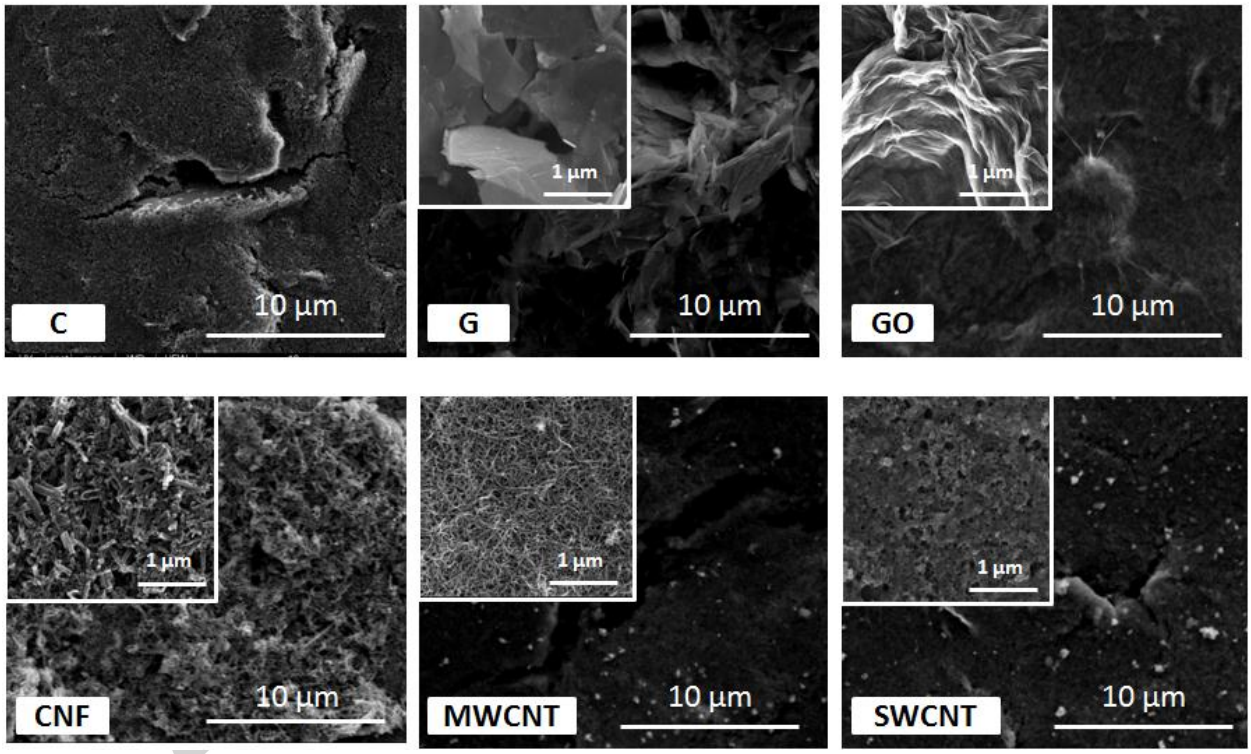

Fig. 2

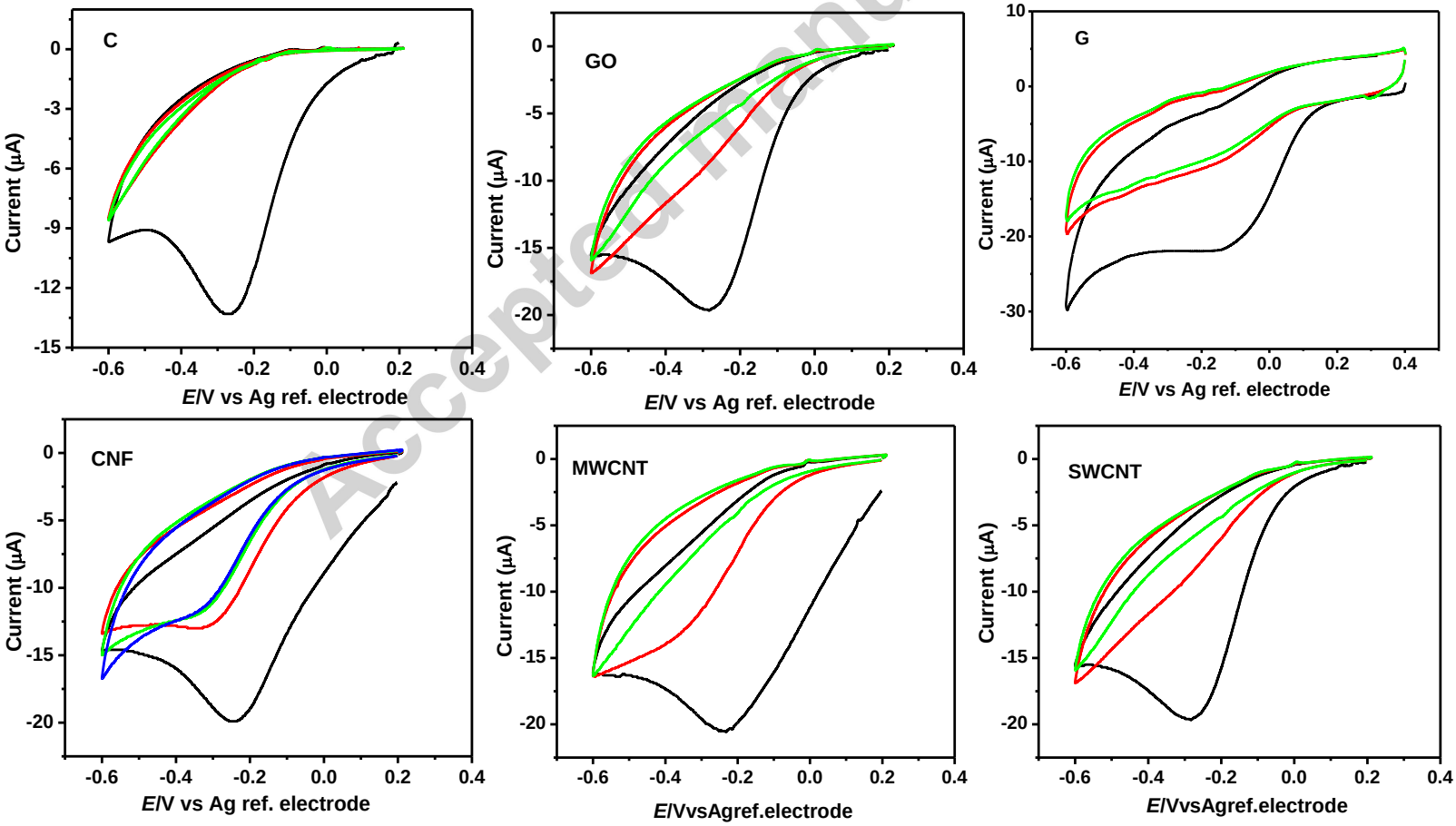

Fig. 3

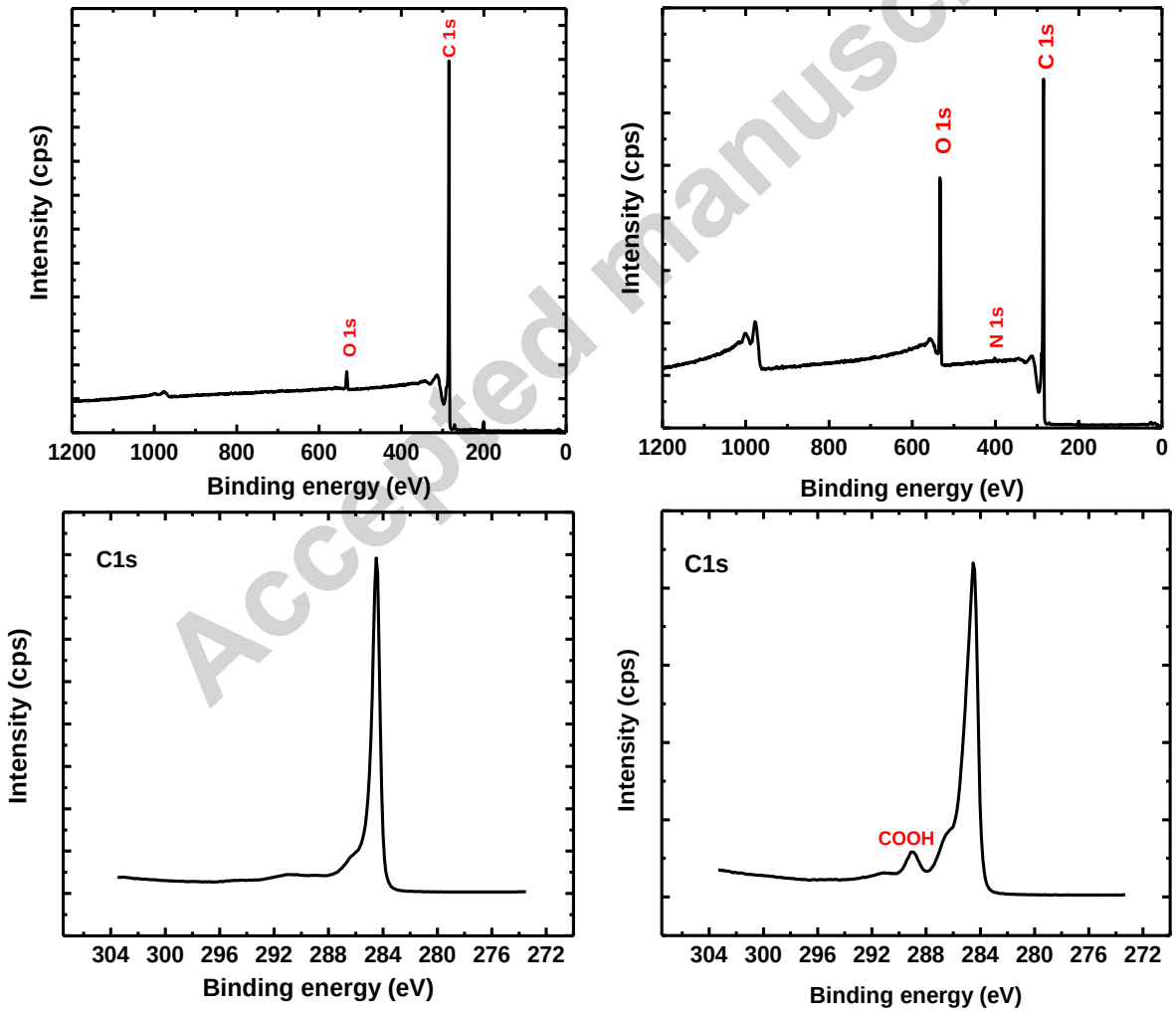

Fig. 4

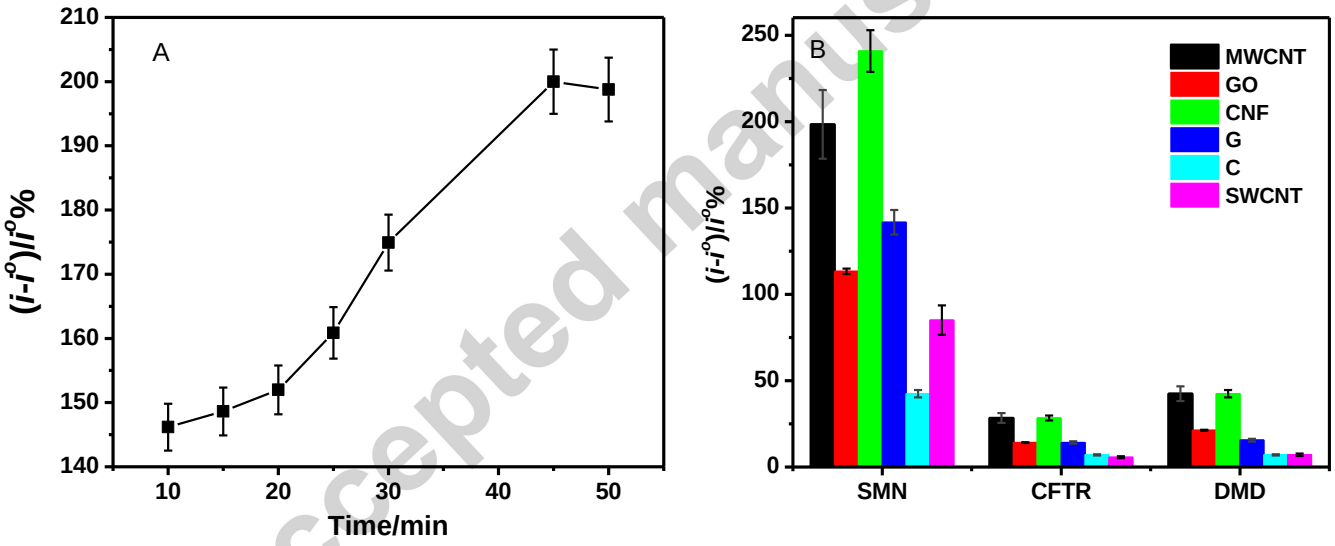

Figure 5

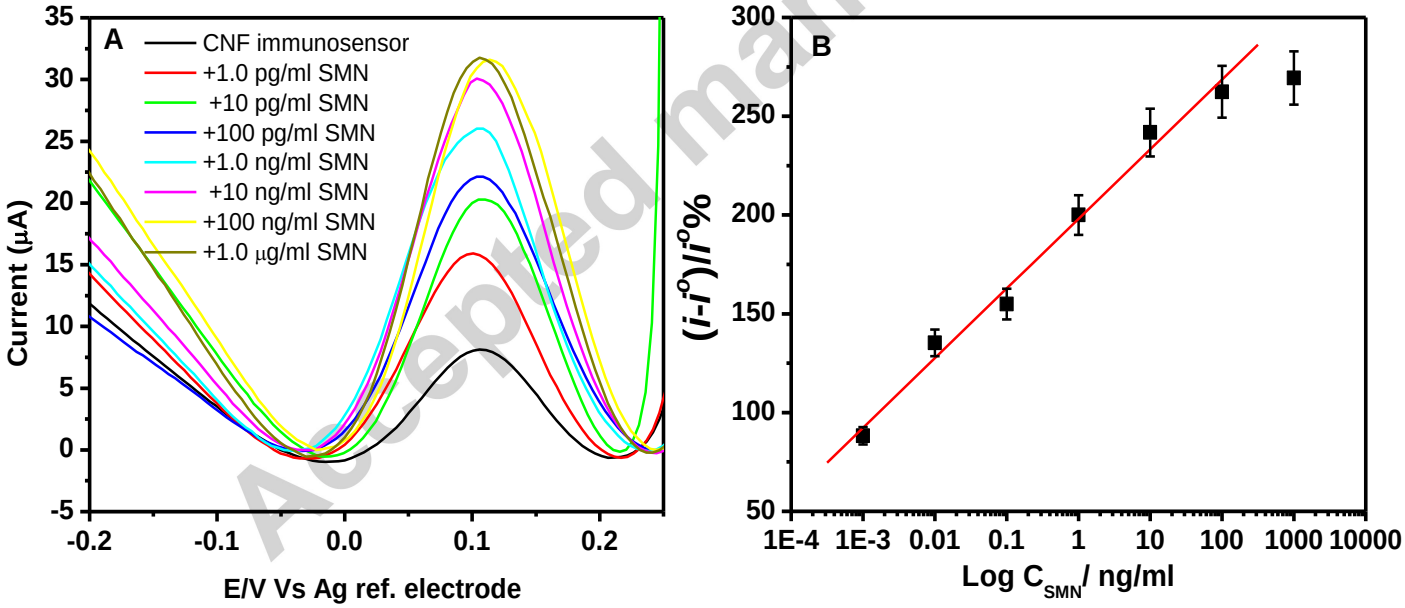

Scheme 1

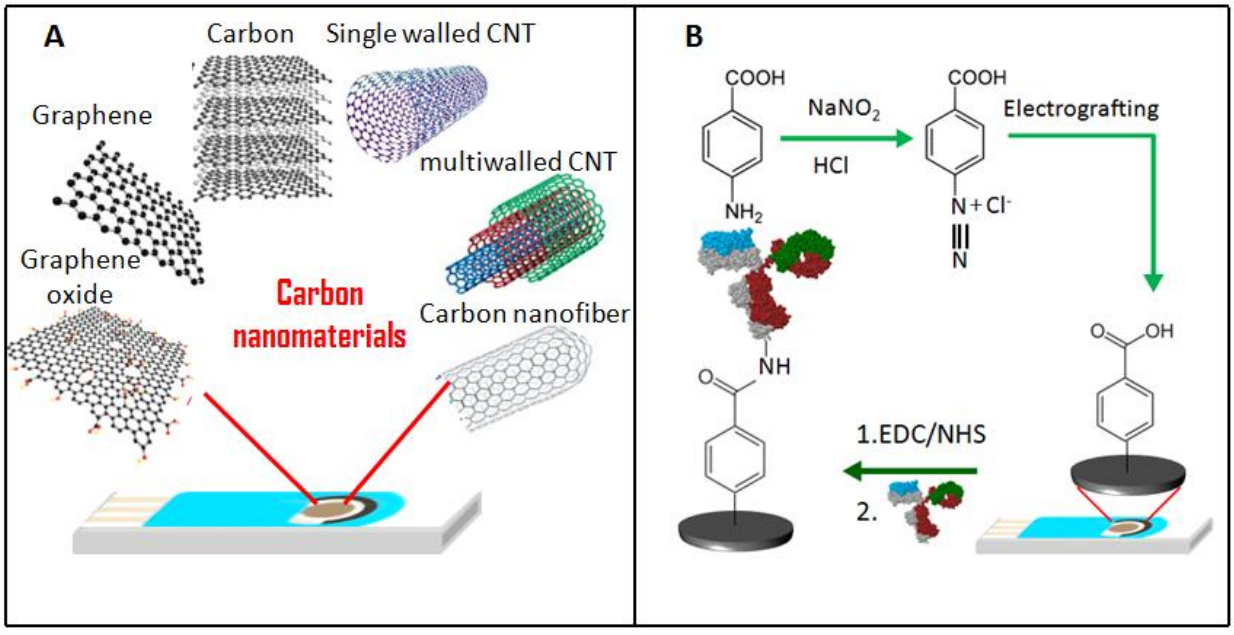

Highlights

- Biosensors for the detection of Spinal muscular atrophy has been developed
- Voltammetric immunosensor for the detection of SMN protein based on covalently functionalized carbon nanofiber-modified screen printed electrodes.
- A comparative study of six different carbon nanomaterial-modified electrodes was performed.
- The detection limit was detection limit of 0.75 pg/ml